Effect of long cyclic exchanges on the magnetic properties of bcc ³He

Ladir Cândido,[1,2] G.-Q. Hai,[2] and D. M. Ceperley[3]

[1]*Instituto de Física, Universidade Federal de Goiás, 74001-970 Goiânia, Goiás, Brazil*
[2]*Instituto de Física de São Carlos, Universidade de São Paulo, 13560-970 São Carlos, São Paulo, Brazil*
[3]*Department of Physics and NCSA, University of Illinois at Urbana-Champaign, Urbana, Illinois 61801, USA*

Using path-integral Monte Carlo calculations, we have calculated ring exchange frequencies in the bcc phase of solid ³He for densities from melting to the highest stable density. We evaluate 42 different exchange frequencies from two atoms up to eight atoms and find their Grüneisen exponents. Using a fit to these frequencies, we calculate the contribution to the Curie-Weiss temperature, Θ_{CW}, and upper critical magnetic field, B_{c2}, for even longer exchanges using a lattice Monte Carlo procedure. We find that contributions from seven- and eight-particle exchanges make a significant contribution to Θ_{CW} and B_{c2} at melting density. Comparison with experimental data is given.

PACS number(s): 67.80.D−, 05.10.Ln, 67.30.−n

I. INTRODUCTION

The magnetic properties of solid ³He have attracted much attention over the last four decades because at millikelvin temperatures, solid ³He is an almost pure spin-1/2 fermion system with a simple crystal structure. The large amplitude of its zero-point motion induces exchanges among the atoms; their frequencies determine the magnetic properties and give rise to a rich magnetic phase diagram. Because of the simplicity of the atomic interaction, it is possible to determine the spin Hamiltonian from first principles and thereby to confront experiment with theory without any adjustable parameters. Hence, this is a very important model with applications to other physical systems. However, it is quite challenging to treat such a highly quantum spin system even with modern computational capabilities.

Following on Dirac,[1] Thouless[2] elucidated the relation between exchange of ³He atoms and the nuclear magnetism of solid ³He. He showed how a spin Hamiltonian results from ring exchanges among ³He atoms. According to this theory, at low temperatures the spins are governed by a Hamiltonian of the form

$$\mathcal{H}_{spin} = -\sum_P (-1)^P J_P \hat{\mathcal{P}}_{spin}, \qquad (1)$$

where the sum is over all cyclic permutations P of atoms, $J_P > 0$ is an exchange frequency, the $\hat{\mathcal{P}}_{spin}$ is the corresponding spin-exchange operator, and $(-1)^P$ is the sign of the permutation: an exchange of an even number of atoms is antiferromagnetic and an odd number of atoms is ferromagnetic.

Above the solidification density ($v = 24.23$ cm³/mole), ³He crystalizes into a body-centered cubic (bcc) structure until the higher density ($v = 19.85$ cm³/mole), when it transforms into an hcp lattice. The bcc lattice is bipartite, so if exchange were only between pairs of nearest-neighbor atoms, the above spin Hamiltonian would reduce to the nearest-neighbor Heisenberg model and the ground state would be antiferromagnetic. However, this is not consistent with experiments.[3] The state at magnetic fields less than 0.4 T and temperatures less than 1 mK is found experimentally to be the U_2D_2 structure, having two planes of up-spins and two planes of down-spins. At higher magnetic field, the system transforms into the canted-normal antiferromagnetic (CNAF) phase. At the upper magnetic field $B_{c2}(v)$ the system transforms into a spin-polarized phase having the same order as the high-temperature paramagnetic phase. A discussion of the history of solid ³He, the exchange model, and its application to other physical systems is given in two recent reviews.[4,5]

Roger, Hetherington, and Delrieu introduced the multiple-spin exchange (MSE) model.[3] In this model, one also considers exchange between three and four atoms. By adjusting the frequencies to some features of the experimental data, they were able to understand the observed spin ordering, the ground-state U_2D_2 structure, the high-temperature specific heat coefficient, and the mean spin-wave velocity. Roger[6] also performed approximate Wentzel-Kramers-Brillouin (WKB) calculations for the exchange frequencies and found that exchanges of two, three, and four particles have the same order of magnitude. This leads to spin frustration because of the competition between exchanges containing an odd or an even number of atoms.

A much more accurate Monte Carlo procedure to calculate the exchange frequencies was introduced by Ceperley and Jacucci[7] (referred to as CJ below). The results were in rough agreement with the empirically determined values and even better agreement with the experimental data. Godfrin and Osheroff[8] (called GO below) then used the MSE model with the CJ exchange frequencies, within the $T = 0$ mean-field approximation to study magnetic properties of the U_2D_2 and CNAF phases of the ³He considering from two- up to six-atom exchange. There are difficulties in testing the MSE model more precisely due to statistical errors of the CJ calculation and the lack of values for higher-order exchanges. For example, it has been suggested that in high magnetic fields (e.g., 20 T) exchanges of more than six spins contribute.[9]

In this paper, we address the contribution of longer exchanges. We want to determine how quickly the exchanges converge if they do, in fact, converge. In doing so we can assess how well first-principles calculations can describe the magnetic properties of solid helium. We report here higher-accuracy Monte Carlo exchange-frequency calculations for bcc ³He including up to eight-atom exchanges at different densities. The exchange-frequency calculations have been

determined to better than 5% accuracy. We estimate finite size corrections and time-step errors for the first time. The corrected frequencies are fit to a formula, allowing us to estimate the exchange frequency for any exchange and thus definitively take into account very long exchange cycles. We then examine the convergence of properties versus cycle length.

We note that the problem of long exchange cycles is relevant to other systems that are more complex than bcc ^{3}He. For example, supersolidity in commensurate solid ^{4}He is determined by long ring exchanges.[10] The same path-integral methods have been used for that problem as well,[11] showing that long ring exchanges are not possible in a perfect helium crystal. However, it is still very unclear what is giving rise to the experimentally observed anomalous dynamic response in solid ^{4}He. A related physical system is ^{3}He absorbed on various substrates, forming a two-dimensional (2D) crystal. The systems might show complex novel phases, but both the calculations[12] and experiments[13] are much more difficult. Finally, exchange frequencies have been calculated for both the 2D (Ref. 14) and three-dimensional (3D)[15] Wigner crystal, the low-density phase of the electron gas. While the 3D Wigner crystal has the conventional antiferromagnetic magnetic order, path-integral Monte Carlo (PIMC) calculations predict the 2D system will form a spin liquid magnetic ground state. Thus, confrontation between theory and computation on bcc ^{3}He can give confidence in the results for other physical systems.

In the next section, we give some details of the computational approach and tests that we have done to establish the accuracy. After that we describe the results and compare to experiment.

II. COMPUTATIONAL APPROACH

The PIMC method for calculating exchange frequencies in quantum crystals is based on the ratio

$$f_P(\beta) = \frac{\langle Z|e^{-\beta H}|PZ\rangle}{\langle Z|e^{-\beta H}|Z\rangle}, \qquad (2)$$

where Z represents the many-body configuration where each atom is on the site of a perfect lattice and PZ is a permutation of the mapping of the atoms to lattice sites. The denominator is the quantum partition function for the distinguishable particle system (Boltzmann statistics) at an inverse temperature β. Assuming the exchange energies are much smaller than phonon energies, an exchange frequency, J_P, is related to f_P by

$$f_P(\beta) = \tanh[J_P(\beta - \beta_{0P})], \qquad (3)$$

for $\beta > \beta_{0P}$ where β_{0P} is the amount of imaginary time to accomplish the exchange P. The ratio f_P is determined by the path-integral Monte Carlo method and then Eq. (3) is inverted to estimate J_P.

In this path-integral algorithm, one does simulations with two types of paths: paths beginning and ending at the perfect lattice positions [the denominator of Eq. (2)] and paths beginning at Z and ending at PZ [the numerator of Eq. (2)]. The imaginary time density matrices $e^{-\beta H}$ are expanded out into a discrete path integral connecting the end points of the paths using an approximate action with a time step τ. Under

the polymer isomorphism, f_P is related to the free energy needed to induce a specific cross-linking, corresponding to the permutation P, into a crystal of ring polymers. Using the Bennett method,[7,16] we directly determine the ratio f_P by matching histograms of the change in action in mapping paths of one type into paths of the other type. We can determine very small values of f_P, and hence J_P, to a relative accuracy of a few percent. The details of the method have been given in an earlier paper[17] including several important improvements over the original method. The method was developed with computer capabilities many orders of magnitude smaller than what is presently available and to examine individual small cyclic exchanges. On current computers we can examine much larger exchanges; however, it is possible that different algorithms could be used to advantage to treat large numbers of large cyclic exchanges.

Helium is unique among the elements in how well its interaction is described by a pair potential. The use of a semiempirical pair potential gives an error in the ground-state energy of less than 1%. We have used the semiempirical Aziz two-body potential[18] and the exact pair action.[10] Note that the earlier CJ calculation used a different potential,[19] one with a different repulsive core. The observed agreement between the present and previous calculations is a test of how sensitive the results are to the potential.

We now discuss the various errors arising in these calculations. In addition to statistical errors, there are systematic errors from the temperature, the time step, and the number of atoms in the periodic box.

A. The statistical error

The dominant error in our calculations is the statistical error. This error is estimated by breaking the computer run into subsets and finding the fluctuation in the estimate of J_P. The statistical error can be reduced by averaging over more PIMC steps or by independent runs on separate computer processors.

B. The temperature bias

Temperature or its inverse, β, enters in this method in Eq. (2) as a parameter. Physically we have to ensure that thermal phonons do not influence the exchange frequencies. This implies that the temperature has to be smaller than the Debye temperature. Note that the Debye temperature for bcc ^{3}He at melting[20] is 19 K. It is not important that we choose a temperature on the scale of the millikelvin temperature at which helium magnetically orders. The most important restriction on β is that it has to be greater than β_0, the imaginary time of the exchange as given in Eq. (3). We estimate β_0 in the calculation and find that it is weakly dependent on the exchange and varies from 0.35 K^{-1} for $p = 2$ to 0.55 K^{-1} for $p = 8$; here p is the number of exchanging atoms.

In order to judge the effect of temperature, we have performed calculations of the two-atom exchange frequency (which is the largest exchange frequency) at five different temperatures for a system with 128 atoms near the melting volume, $v = 24.12$ cm^3/mole. The results are shown in Fig. 1. The observed temperature dependence for 128 atoms is well fit by the expression $J_{1N}(T) = J_{1N}(0) + \eta T^3$.
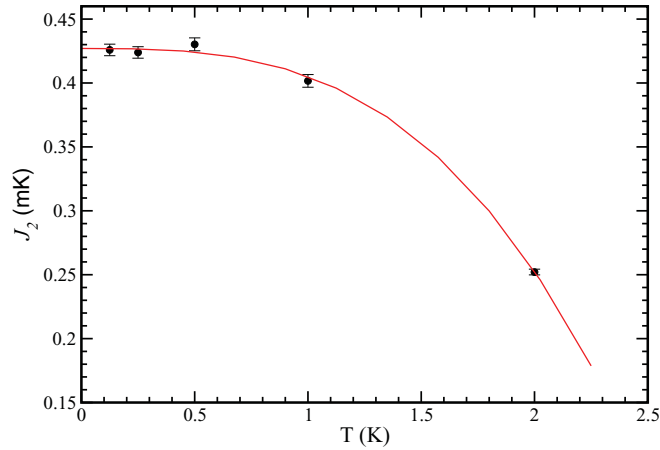
FIG. 1. (Color online) Temperature dependence in the PIMC calculations for J_{1N} (the two-particle nearest-neighbor exchange) at $v = 24.12$ cm^3/mole for systems with $N = 128$ atoms. The red curve is a nonlinear least-squares fit to the PIMC data: $J_{1N}(T) = J_{1N}(0) + \eta T^3$.

Because the Debye temperature increases with decreasing molar volume, a system at smaller volume should reach its convergence at higher temperature. We therefore conclude that, for $T \leqslant 0.5$ K, temperature effects are negligible at all densities. All the following calculations use $T = 0.5$ K and $\beta = 2$ K^{-1}.

C. The time-step error

Next, we study how the exchange frequencies depend on the time step τ of the approximate action. Trotter's formula ensures that if τ is sufficiently small the quantum integrals will be computed exactly; the rate of convergence depends on the quality of the action. The present calculations use tables of the exact action for pairs of atoms. The discretization only has to correct for effects of three or more bodies. Figure 2 shows the time-step dependence for exchanges involving two, three, and four atoms. The results are fit to the expression $J_P(\tau) = J_P(0) + \xi \tau^5$. The exponent 5 reflects the high quality of the pair action. We see that for $\tau \leqslant 0.025$ K^{-1} the exchange frequencies are practically independent of the time step. One expects that since higher-body exchanges keep atoms farther apart during exchange, time-step errors would be largest for the two-body exchange. We use $\tau = 0.025$ K^{-1} in the subsequent calculations. Hence, using the temperature as determined above, the exchange process has 80 discrete steps.

D. The size effect

Finally, we study how the exchange frequency depends on the number of atoms, N, in the simulation cell. As is typical in most simulations, periodic boundary conditions are used to eliminate most effects of finite N. The bcc lattice is consistent with cubic boundary conditions; the number of lattice sites is taken to be twice the cube of an integer, starting at 128 and going up to 1024.

The main effect on the exchange frequency of the finite system size comes from the highly nonlinear dependence of the exchange frequency on density. If a zero-point phonon, with
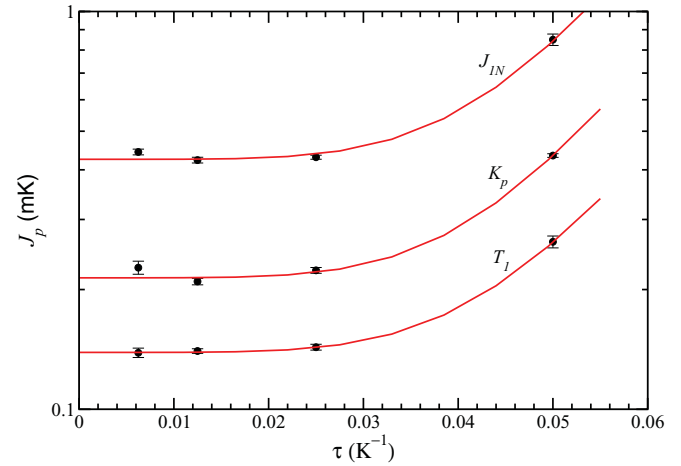

FIG. 2. (Color online) The dependence of the estimated exchange frequency on the time step for the most important two-, three-, and four-particle exchange frequencies at $v = 24.12$ cm^3/mole for systems with $N = 128$ atoms.

wavelength greater than several lattice constants, is present, in regions of enhanced (decreased) density the exchanges are suppressed (enhanced). However, in a finite simulation cell, the maximum wavelength equals the box size. Since the exchange frequency is highly dependent on the local density, ρ, and $J \sim \rho^{-\Gamma}$ where $15 < \Gamma < 30$, cutting off the long-wavelength phonon spectrum makes exchange more difficult and reduces the average exchange frequency.

We have investigated the size dependencies of the most important exchanges from two to six atoms by varying the number of atoms in the cell from 128 up to 1024 as shown in Fig. 3 near melting. We find that the exchange frequencies can be described by $J_P = J_P(\infty) + \zeta_P/N$. The corrections for five- and six-body exchanges are negligible within statistical error, as are all size corrections for exchange frequencies with $J_P < 0.1$ mK. Figure 4 shows the size effect near the high-pressure limit of the bcc solid, $v = 20.07$ cm^3/mole. For
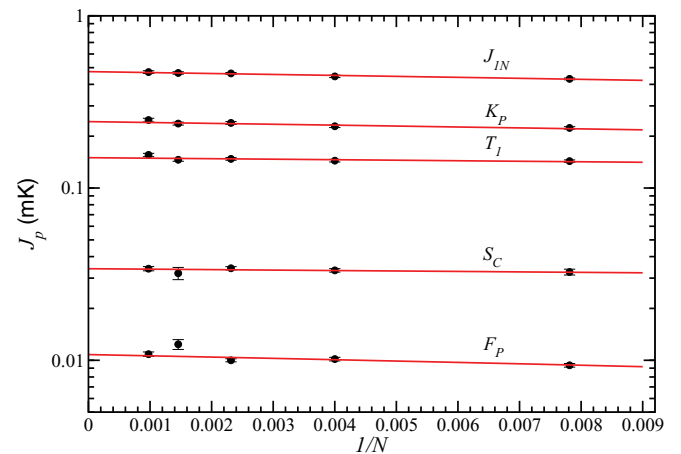

FIG. 3. (Color online) Dependence of the exchange frequency on the number of atoms in the cell, N, for most important 2, 3, 4, 5 and 6 particle exchanges at the volume $v = 24.12$ cm^3/mole, $\tau = 0.025$ K^{-1} and $T = 0.5$ K. The red curve is a fit to the PIMC data.
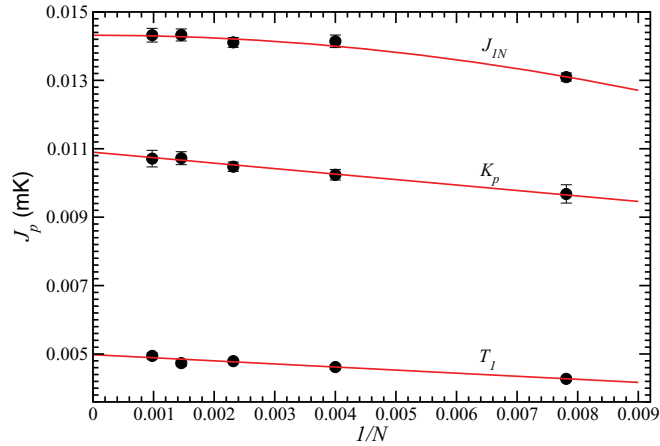
FIG. 4. (Color online) Size dependence for the important two-, three-, and four-particle exchange frequencies at $v = 20.07$ cm^3/mole. The red curve is a fit to the PIMC data.

two-body exchange at this density, we need terms using both N^{-1} and N^{-2}. At the highest pressure, the size correction is insignificant for $J_P < 1\,\mu$K.

III. CALCULATED EXCHANGE FREQUENCIES

We have performed PIMC calculations of the exchange frequencies from two- up to eight-atom cyclic exchanges at different densities. Some of the exchanges considered are shown in Table I. They include all possible ring

exchanges involving two, three, and four atoms with nearest- or next-nearest-neighbor "hops." We have calculated the 10 most important five-atom exchange frequencies, the 18 most important six-atom exchanges, as well as some important eight-atom exchange frequencies. We selected these longer exchanges by performing random walks on a bcc lattice, as explained below.

We use the notation for the exchanges from Refs. 3 and 8. We label distances between nearest neighbors as 1, next-nearest neighbor as 2, etc. For a p particle cyclic exchange, the first p numbers are the distances between successive sites on the exchange; thus we write a six-particle exchange between nearest neighbors as $\{111111\}$ or more succinctly as $\{1^6\}$. The next group of integers (separated by a semicolon) gives the p distances between atoms that are two atoms apart on the cycle. The next set of numbers would give the distances between atoms three apart on the cycle, etc. Although the notation does not always map onto a single exchange, in almost all cases one can work out the specific cycle with this notation. In addition, some of the smaller exchanges are given symbols and names, in agreement with the previous literature, in particular Godfrin and Osheroff,[8] who give explicit diagrams of the exchanges.

Figure 5 shows our estimates of the three most important exchange frequencies as a function of molar volume. It is evident that they scale with density as

$$J_P(v) = J_P(v_0)(v/v_0)^{\Gamma_P}, \qquad (4)$$

where Γ_P is the so-called Grüneisen parameter. Table II gives the size-corrected exchange frequencies at the reference volume: $J_P(v_0)$ and Γ_P. Note that the three largest exchanges,

TABLE I. The exchange frequencies in μK as a function of molar volumes (cm^3) for $N = 128$ atoms. The digits in parentheses are the estimated standard errors in the last decimal place.

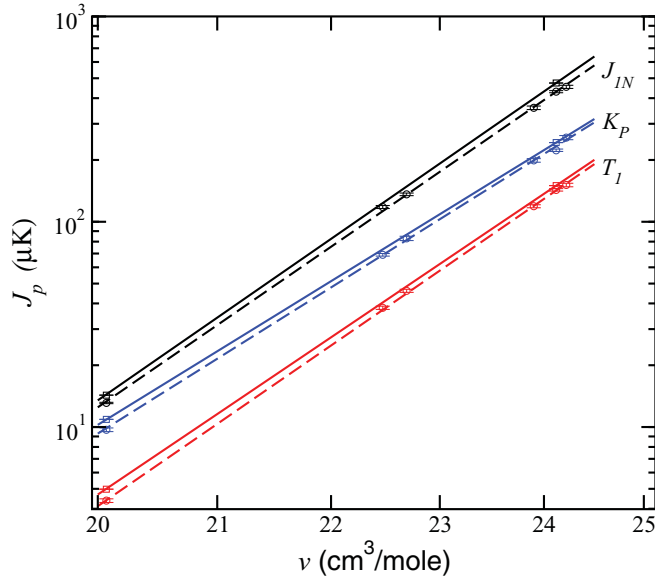| p	Exchange	Name	20.07	22.47	22.69	23.90	24.12	24.22
2	(11)	J_{1N} (NN)	13.1(1)	118(2)	136(2)	359(7)	430(5)	454(8)
	(22)	J_{2N} (NNN)	0.84(2)	11.8(3)	15.8(3)	52(1)	63(1)	67(2)
	(33)	J_{3N} (NNNN)						0.11(3)
3	(112)	T_1 (triplet)	4.38(9)	38.1(7)	46.1(8)	119(2)	143(2)	151(3)
	(113)	T_2	0.0163(3)	0.42(1)	0.60(2)	2.56(7)	3.41(9)	3.7(1)
4	$(1^4;23)$	K_P (planar)	9.7(2)	69(1)	83(2)	199(4)	223(3)	257(6)
	$(1^4;22)$	K_F (folded)	0.403(7)	5.70(9)	6.9(1)	23.0(5)	27.2(6)	30.7(6)
	(1212;14)	K_L (lozenge)	0.118(3)	1.91(3)	2.39(5)	8.4(2)	10.6(2)	11.4(3)
	(1122;31)	K_A (diamond)	0.0498(8)	1.04(3)	1.26(3)	4.8(3)	6.3(1)	6.6(1)
	$(2^4;33)$	K_S (square)	0.0207(5)	0.46(2)	0.55(2)	2.32(8)	3.01(5)	3.2(1)
	(1212;11)	K_B (eight)					0.76(2)	
5	$(1^42;52341)$	F_1 (planar)	0.104(3)	1.690(6)	2.18(7)	7.6(2)	9.4(2)	10.2(3)
	(11211;24133)	F_2	0.054(1)	1.01(2)	1.28(3)	4.9(1)	6.2(2)	6.6(2)
	(11211;24132)	F_3	0.0116(3)	0.316(9)	0.40(1)	1.8(1)	2.20(8)	2.42(8)
	(22122;34243)	F_4					0.125(4)	
6	$(1^6;3^6;4^3)$	S_1 (crown)	0.72(1)	7.3(2)	8.8(3)	26.3(9)	33(1)	36(1)
	$(1^6;253253;471)$	S_2 (planar)	0.125(4)	1.84(6)	2.50(7)	8.5(3)	10.7(4)	12.0(5)
	$(1^6;233323;144)$	S_3	0.023(1)	0.50(1)	0.66(2)	2.8(1)	3.6(2)	4.0(2)
	$(1^6;332323;414)$	S_4	0.024(1)	0.53(2)	0.63(2)	2.7(1)	3.3(1)	4.0(2)
	$(21^42;433343;544)$	S_5	0.0177(5)	0.41(2)	0.54(2)	2.0(1)	2.5(1)	3.1(2)
	$(1^6;325223;144)$	S_6	0.0094(3)	0.25(1)	0.35(3)	1.53(6)	1.96(8)	2.06(8)
	$(1^6;322523;414)$	S_7					1.90(8)	
8	$(1^8;(5222)^2;(7117)^2;2626)$	O_1	0.0138(5)	0.28(1)	0.40(2)	1.40(6)	1.94(8)	2.4(2)

FIG. 5. (Color online) Density dependence of the largest two-, three-, and four-atom exchange frequencies for $N = 128$ (the circles and dashed lines) and for $N = \infty$ with sized corrections (the squares and solid lines).

J_{1N}, T_1, and K_P, have $17 \leqslant \Gamma_P \leqslant 19$, the six-cycle crown exchange has $\Gamma_P = 21$, while all the other exchanges have $23 < \Gamma_P < 29$. As the density increases, the first four mentioned exchanges become dominant. This is in accordance with the measurements by Fukuyama et al.[21] and the estimate of the action by Roger[6] using a WKB method.

TABLE II. The estimated frequencies at $v_0 = 24.12$ cm³/mole and the Grüneisen exponent Γ_P. Also shown are the previous PIMC results (J_{CJ}) from Ref. [7] as reported in Ref. [8]. The digits in parentheses are the estimated standard errors in the last decimal place.

p	Name	J_{CJ}	$J_P(v_0)$ (µK)	Γ_P
2	J_{1N}	453(32)	474(5)	19.0(2)
	J_{2N}	62(6)	63(1)	23.4(2)
3	T_1	182(20)	150(2)	18.5(1)
	T_2	5.3(1)	3.36(9)	29.0(2)
4	K_P	250(25)	243(4)	16.9(2)
	K_F	32(5)	28.1(6)	23.0(2)
	K_L	11(3)	10.5(2)	24.4(1)
	K_A	6(2)	6.2(1)	26.1(3)
	K_S	1.9(6)	2.95(5)	26.9(2)
5	F_1	5.3(1)	9.5(2)	24.5(1)
	F_2		6.1(2)	25.7(1)
	F_3		2.26(8)	28.5(3)
6	S_1	34(10)	32(1)	20.8(2)
	S_2	10(3)	10.7(4)	24.2(2)
	S_3		3.6(2)	27.5(1)
	S_4		3.4(1)	27.0(3)
	S_5		2.6(1)	27.1(4)
	S_6		1.95(8)	29.0(3)
8	O_1		1.97(8)	27.0(5)

Also shown in Table II are the previous PIMC estimates of exchange frequencies. In general, the agreement with the previous calculation is very good in spite of the difference between that calculation and the present one. The main difference is the magnitude of the statistical error. Also those calculations were for $N = 54$, they did not include size corrections, and the helium interaction was different.

In order to estimate the effects of longer exchange cycles, we compute the frequencies of 6 different five-atom exchanges, 11 different six-atom exchanges, and 6 different eight-atom exchanges at the molar volume 24.12 cm³/mole. These results are not shown in Table I. We then fit all of the exchange frequencies to the expression

$$J_P = \exp(a_0 + a_1 n + a_2 m + a_3 c), \qquad (5)$$

where n and m are the number of first- and second-neighbor hops in the exchange (with $p = n + m$), $c = \sum_i^p (1 + \hat{\mathbf{d}}_i^+ \cdot \hat{\mathbf{d}}^-)^2$, and $\hat{\mathbf{d}}_i^\pm$ is the unit vector from site i on the exchange to the nearby sites in the two exchange directions. The parameters a_1 and a_2 measure the increase in action in adding a nearest- or next-nearest-neighbor "hop" to an exchange cycle. On the other hand, a_3 favors straight exchanges versus ones that double back on themselves; if the exchange angle is acute, it is likely that the incoming and outgoing atoms will collide, thus decreasing the exchange frequency. This expression for the action was found by Ceperley and Bernu[11] to provide a good fit to exchange frequencies of solid ^{4}He. For ^{3}He at this density, it fits the exchange frequencies to a relative error of 12% accuracy over our database of 42 different computations. Figure 6 shows the comparison between the PIMC frequencies and the fitted frequencies. We excluded from the fit the pair exchanges and exchanges beyond next-nearest neighbors, e.g., all J_n's and T_2. At the melting density, we find the best fit parameters are $\exp(a_0) = 3.27$ K, $a_1 = -1.702$, $a_2 = -2.826$, and $a_3 = -0.640$ with errors on a_1, a_2, and a_3 less than 1%. By using the 16 frequencies at 20.07 cm³, we estimate the
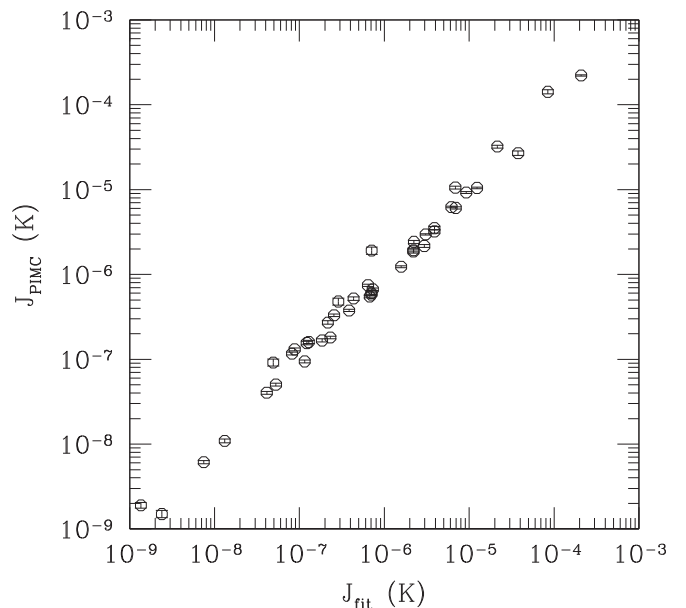

FIG. 6. Comparison of the fitted expression Eq. (5) with the 42 PIMC determined frequencies with error bars.

Grüneisen parameters of the fitting coefficients ($\partial a_k/\partial \ln v$) to be $(-8.3, 4.0, 6.7, 2.1)$, respectively.

IV. CALCULATION OF MAGNETIC PROPERTIES

Having determined the exchange frequencies in Table II, and using the fit for exchanges not in Table II, we can study the magnetic properties based on the spin Hamiltonian, Eq. (1).

Previous work, for example, the MSE model, has assumed that only a few frequencies contribute to experimental properties. We wish to establish, from first principles, the extent to which longer exchanges are important. We are in a position to do so because the fit to the 42 exchange frequencies allows an estimate of the frequency of all cyclic exchanges. However, note that we restrict consideration to cyclic exchanges composed of nearest- or next-nearest-neighbor hops.

It is not feasible to analyze by hand relevant cycles as has been done in the past, because the number of possible cycles grows rapidly with exchange length. Instead, we sample random walks on the lattice and thereby obtain a Monte Carlo (MC) estimate of some of the measured properties, in particular, the Curie-Weiss temperature Θ_{CW} and the value for the upper critical magnetic field, B_{c2}. We choose these quantities to compute because each is a linear function of the exchange frequencies, making the MC estimate straightforward, and because experimental measurements are available.

The procedure to perform the random-walk estimate of these quantities is as follows. The random walk on the bcc lattice is started at the origin, and one of the 14 possible "hops" to a neighboring site is chosen at random (8 nearest- plus 6 next-nearest-neighbor sites). The random walk continues until either the walk revisits one of the previously visited lattice sites, or the walk is too long (has more than 20 hops). Walks that return to the origin before they hit any of the other visited sites are counted in the statistics, while all other walks are discarded. Let p be the number of hops of a useful walk with permutation P. The contribution of that walk is then $14^p J_P$. The exchange frequency is either evaluated from Eq. (5) or for the exchanges in Table II, that table value is used. We used the exponents in Table II to scale to different densities; for frequencies not in this table we used the estimated Grüneisen exponents of the fitted parameters. Importance sampling could be used to make the procedure more efficient; however, enough precision could be easily obtained with the simple procedure outlined above. Using the lattice MC algorithm, we reproduced the results of GO[8] with the CJ frequencies; those results involved explicit counting of exchanges and group theory analysis of their effect on properties.

To characterize the overall contribution of cycles of various lengths, we computed the contribution to the ferromagnetic energy of cycles of length p: $A_p = -(-14)^p \langle J_P \rangle$, where the brackets indicate averaging over the lattice walks. Observable properties are a function of A_p, as we discuss below. In the results reported, 2×10^{10} lattice walks were used so that the error due to the lattice walk statistics was very small. Values of A_p at high and low density are shown in Fig. 7. We see there is a fairly slow decay at the melting density but a much faster decay at high density. The high-density exchanges are clearly dominated by the small exchange cycles. The slow decay at
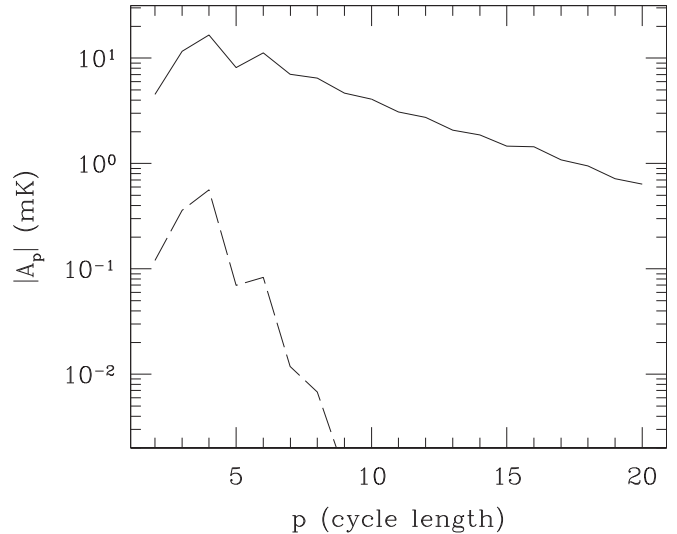

FIG. 7. Convergence of the contribution of exchange frequencies of a given cycle length at molar volume 24.22 cm³ (solid line) and at a smaller volume 20.07 cm³ (dashed line).

melting density comes about because the rapid decay of the exchange frequencies is partially offset by the rapid increase in the number of exchanges. We note that because even and odd exchanges have opposite signs, the effect of long exchanges on physical properties converges much faster.

A. Estimate of Θ_{CW}

We define the partial Curie-Weiss temperature θ_p as the contribution to Θ_{CW} coming from exchange cycles of length p. Hence $\Theta_{CW} = \sum_p \theta_p$. It is related to A_p by

$$\theta_p = (p-1)2^{-p+1} A_P \tag{6}$$

and is given in Table III at the melting density.

At the melting volume we calculate $\Theta_{CW} = -1.98 \pm 0.1$ mK. The experimental estimates range from -1.7 to -2.0 mK, in agreement with the present calculations.[22] Figure 8 shows the convergence of Θ_{CW} versus

TABLE III. Contributions to Θ_{CW} and to magnetization for exchange cycles of length p for $v = 24.22$ cm³/mole.

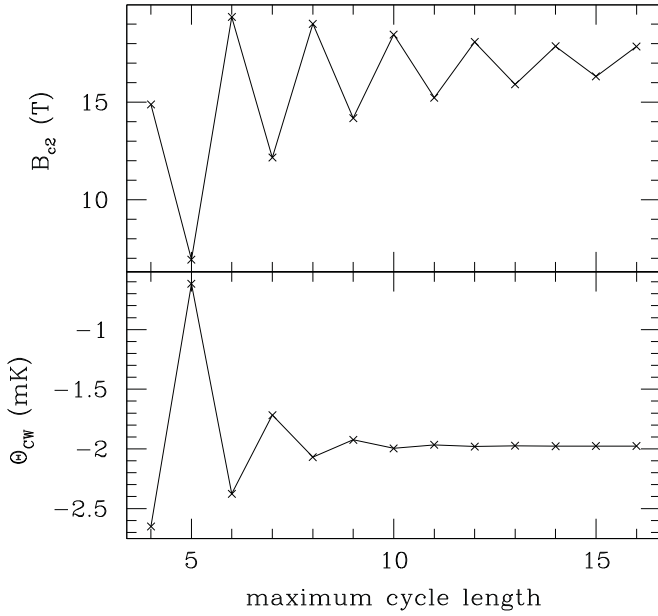| p	θ_p (mK)	x_p (mK)
0		0.228
1		-1.333
2	2.26	2.592
3	-5.83	0.652
4	6.22	0.143
5	-2.03	0.039
6	1.76	0.016
7	-0.66	0.007
8	0.35	0.013
9	-0.153	0.002
10	0.061	
11	-0.027	
12	0.013	

FIG. 8. Convergence of the Curie-Weiss temperature and the upper critical field vs the maximum cycle length at molar volume 24.22 cm^3.

the maximum cycle length. We note that the contribution from nine cycles is 0.15 mK (Table III). However, there is substantial cancellation between even and odd cycles, so the convergence is effectively reached after seven cycles. Figure 9 compares the theoretical and measured values of Θ_{CW} as
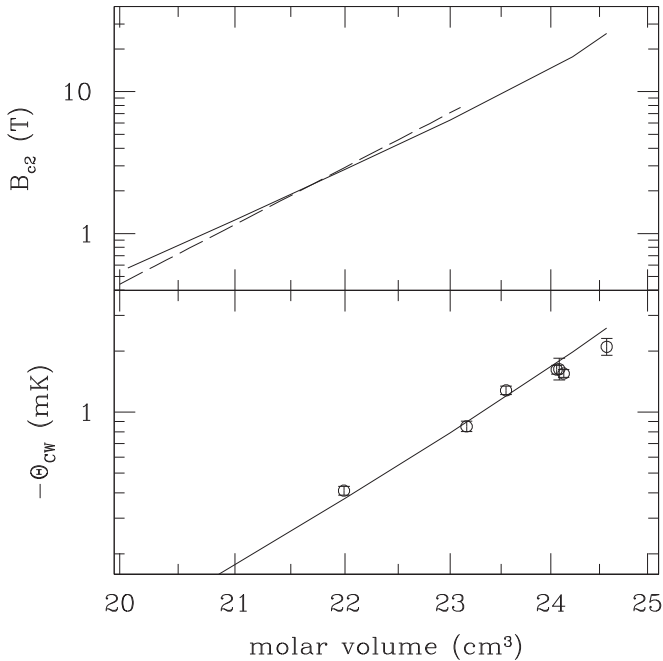

FIG. 9. Comparison of theory with experiment for the upper critical field (top) and the Curie-Weiss temperature (bottom) vs molar volume. In the top panel the dashed line represents the experimental estimates[9] and the solid line the PIMC estimates. In the bottom panel, the line represents the PIMC estimate and the open symbols with error bars the measurements.[22] Note that we have matched the experimental measurements of Θ_{CW} with the PIMC ones at the molar volume 21.07 cm^3.
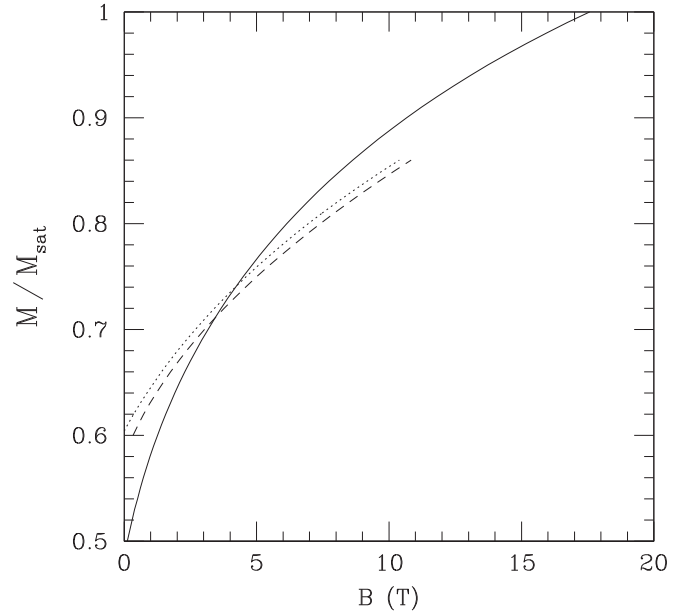

FIG. 10. Comparison of the theoretical magnetization (solid curve) vs the experiment measurements (dotted[23] and dashed curves[21]) at $v = 24.22$ cm^3/mole.

a function of molar volume between 22 and 24 cm^3. The agreement is very good at all densities.

The errors in Θ_{CW} come almost entirely from the PIMC uncertainties in J_P (e.g., from Table I), particularly the statistical errors of the largest exchange frequencies. The errors from the fit for large p and the error due to sampling the lattice walks are an order of magnitude smaller.

B. Estimate of B_{c2} and magnetization

As described by GO,[8] at the mean-field level at zero temperature, the relation between the applied magnetic field (B) and the resulting magnetization (M) in the CNAF phase is

$$B = \frac{4k_B}{\gamma\hbar} \sum_{k=1}^{\infty} k x_k y^{2k-1}, \qquad (7)$$

where $y = M/M_{sat}$ is the fractional magnetization. The coefficients x_k are obtained in the lattice walk as averages:

$$x_k = (-14)^p \langle J_P \delta_{n,2k}/n \rangle. \qquad (8)$$

Here n is the number of nearest-neighbor hops in the permutation P. This formula arises because of the antiferromagnetic structure of the CNAF phase. Every nearest-neighbor exchange costs energy because it puts a spin on the incorrect sublattice; thus it is inhibited by a factor y^n. The upper critical field is given by setting $y = 1$: $B_{c2} = (4k_B)/(\gamma\hbar) \sum k x_k$. Computed values of x_k at the melting density are shown in Table III.

We obtain an estimate for $B_{c2} = 17.6 \pm 1$ T at the melting volume 24.22 cm^3. The experimental estimates[9,23] are between 19.3 and 22.7 T. But we note that existing experimental data are limited to a maximum of 12 T; hence, the experimental B_{c2} is extrapolated from measurements at smaller fields. The comparison between theory and experiment is better at higher

densities because the value of B_{c2} is in the experimentally accessible range, as seen in Fig. 9.

Figure 8 shows the convergence of B_{c2} as a function of the maximum cycle length at the melting density. As others have speculated,[8,9] convergence versus cycle length is very slow. There is an appreciable even-odd effect. However, when the cycles are partially summed to get x_k, the result is a positive number that converges much faster. Only the first four values of x_k are needed, which are determined by up to nine cycles.

Figure 10 shows the comparison between the magnetization curve from theory and measurement.[21,23] Although they cross at around 4 T, they have different slopes. We note that the magnetization formula does not account for quantum fluctuations in the CNAF phase. These could be important for values of magnetic field less than saturation, though they are not important at $M/M_{\mathrm{sat}} = 1$ since polarized systems cannot fluctuate.

V. CONCLUSION

Overall we see important effects of long exchange cycles. More importantly, we have found that it is quite feasible with modern techniques to determine all of the exchange frequencies of solid ^{3}He with enough accuracy to compare directly to experiment. To go further, one has to perform many-body calculations of the exchange Hamiltonian. This later step is particularly challenging in view of the very large number of exchange cycles that contribute, but it could be done with a stochastic technique by further developments of the random lattice walk. The present study gives added confidence in using the Monte Carlo method for other systems where the physics is determined by ring exchanges. In those systems, for example in two dimensions, it will be interesting to see whether the limitation to small exchange cycles goes away.

In the development of the original exchange picture, one imagined that exchanges were localized, proceeding across a handful of low action barriers in phase space. This picture is certainly appropriate at high density. However, a complementary picture, the "liquid drop" model, might be useful near melting. Suppose long-wavelength zero-point phonons combine to create a low-density spot in the crystal. Because the system is near melting, the atoms in this spot will have a mobility equivalent to the liquid. As the phonons move on, the crystal will freeze into a long permutation cycle. In this model, there are many equivalent barriers for exchange in phase space. The rate-limiting step for all exchanges is the creation of the low-density region. Although there is nothing in our results to directly support this model, it could be a useful model for other physical systems and possibly amenable to experimental test.

[1] P. A. M. Dirac, Proc. R. Soc. **123**, 714 (1929); P. A. M. Dirac, *The Principles of Quantum Mechanics* (Clarendon, Oxford, 1947), Chap. IX.

[2] D. J. Thoulesss, Proc. Phys. Soc. London **86**, 893 (1965).

[3] M. Roger, J. H. Hetherington, and J. M. Delrieu, Rev. Mod. Phys. **55**, 1 (1983).

[4] E. D. Adams, J. Low Temp. Phys. **135**, 695 (2004).

[5] M. Roger, J. Low Temp. Phys. **162**, 625 (2011).

[6] M. Roger, Phys. Rev. B **30**, 6432 (1984).

[7] D. M. Ceperley and G. Jacucci, Phys. Rev. Lett. **58**, 1648 (1987).

[8] H. Godfrin and D. D. Osheroff, Phys. Rev. B **38**, 4492 (1988).

[9] H. Fukuyama, K. Yawata, T. Momoi, H. Ikegami, and H. Ishimoto, arXiv:cond-mat/0505177 (unpublished).

[10] D. M. Ceperley, Rev. Mod. Phys. **67**, 279 (1995).

[11] D. M. Ceperley and B. Bernu, Phys. Rev. Lett. **93**, 155303 (2004).

[12] G. Misguich, B. Bernu, C. Lhuillier, and C. Waldtmann, Phys. Rev. Lett. **81**, 1098 (1998).

[13] M. Roger, C. Bäuerle, Yu. M. Bunkov, A.-S. Chen, and H. Godfrin, Phys. Rev. Lett. **80**, 1308 (1998).

[14] B. Bernu, L. Cândido, and D. M. Ceperley, Phys. Rev. Lett. **86**, 870 (2001).

[15] L. Cândido, B. Bernu, and D. M. Ceperley, Phys. Rev. B **70**, 094413 (2004).

[16] C. Bennett, J. Comput. Phys. **22**, 245 (1976).

[17] B. Bernu and D. Ceperley, in *Quantum Monte Carlo Methods in Physics and Chemistry*, edited by M. P. Nightingale and C. J. Umrigar (Kluwer, Dordrecht, 1999).

[18] R. A. Aziz, A. R. Janzen, and M. R. Moldover, Phys. Rev. Lett. **74**, 1586 (1995).

[19] R. A. Aziz, V. P. S. Nain, J. S. Carley, W. L. Taylor, and G. T. McConville, J. Chem. Phys. **70**, 4330 (1979).

[20] D. S. Greywall, Phys. Rev. B **15**, 2604 (1977).

[21] H. Fukuyama, T. Okamoto, T. Fukuda, H. Akimoto, H. Ishimoto, and S. Ogawa, Phys. Rev. Lett. **67**, 1274 (1991).

[22] W. P. Kirk, Z. Olejniczak, P. Kobiela, A. A. V. Gibson, and A. Czermak, Phys. Rev. Lett. **51**, 2128 (1983).

[23] D. D. Osheroff, H. Godfrin, and R. Ruel, Phys. Rev. Lett. **58**, 2458 (1987).